metals

MDPI

Article

Microstructural and Mechanical Response of NiTi Lattice 3D Structure Produced by Selective Laser Melting

Carlo Alberto Biffi *, Paola Bassani, Jacopo Fiocchi and Ausonio Tuissi

National Research Council—Institute of Condensed Matter Chemistry and Technologies for Energy, Unit of Lecco, CNR ICMATE, Via Previati 1/E, 23900 Lecco, Italy; paola.bassani@cnr.it (P.B.); jacopo.fiocchi@icmate.cnr.it (J.F.); ausonio.tuissi@cnr.it (A.T.)

* Correspondence: carloalberto.biffi@cnr.it; Tel.: +39-0341-2350111

Received: 15 April 2020; Accepted: 9 June 2020; Published: 18 June 2020

Abstract: Nowadays, additive manufacturing (AM) permits to realize complex metallic structural parts, and the use of NiTi alloy, known as Nitinol, allows the integration of specific functions to the AM products. One of the most promising designs for AM is concerning the use of lattice structures that show lightweight, higher than bulk material deformability, improved damping properties, high exchange surface. Moreover, lattice structures can be realized with struts, having dimensions below 1 mm—this is very attractive for the realization of Nitinol components for biomedical devices. In this light, the present work regarded the experimental characterization of lattice structures, produced by selective laser melting (SLM), by using Ni-rich NiTi alloy. Differential scanning calorimetry (DSC), electron backscatter diffraction (EBSD), and compression testing were carried out for analyzing microstructure, martensitic transformation (MT) evolution, and superelasticity response of the SLMed lattice samples. The lattice microstructures were compared with those of the SLMed bulk material for highlighting differences. Localized martensite was detected in the nodes zones, where the rapid solidification tends to accumulate solidification stresses. An increase of martensitic transformation temperatures was also observed in lattice NiTi.

Keywords: shape memory alloys; NiTi; selective laser melting; additive manufacturing; lattice structure; EBSD; superelasticity

1. Introduction

Among the advantages offered by additive manufacturing (AM), the design for freedom is probably the most important because it enables the possibility of integrating extra functionalities, geometrically dependent, into the built parts [1]. In this light, AM of smart materials, including shape memory alloys (SMAs), is considered a challenging research topic. Among SMAs, the most widespread one is the intermetallic Ni–Ti, which exhibits two peculiar properties, namely, shape memory effect and superelasticity [2,3]. These properties have promoted the diffusion of nearly equiatomic NiTi alloy in industrial applications, oriented to actuators and a biomedical field [4,5].

Available literature reports several works based on the study of the microstructure of Nitinol parts, manufactured by the most diffused metal AM technologies, including selective laser melting (SLM), direct energy deposition, and electron beam melting [6]. However, most of the achieved results regard the realization of bulk or massive samples [7,8], while only a few are dedicated to the study of thin or lattice structures in Nitinol [9,10]. It is well known from results regarding other alloys, such as Ti6Al4V and CoCrMo, that production of thin parts or lattice structures is associated with reduced processability windows. Moreover, thin structures can be also more sensitive to the correlation between

the thermal gradients, induced during solidification, and the mechanical behavior of the specific alloy. This effect can be associated with the balance between the generation of internal residual stresses, when the massive geometry of the part does not allow their relaxation, and the thermal distortions, which can occur when the slender geometry permits the stress to relieve.

Therefore, due to the high sensibility of Nitinol to both thermal and mechanical fields [11,12], which both may trigger the martensitic transformation [8,13–16], the investigation of the microstructural properties of Nitinol lattice structures appears as a challenging field. The successful development of such research can lead to the potential use of complex 3D printed parts for industrial applications. In the present work, experimental characterization of Ni-rich NiTi lattice structures, produced by SLM, was carried out. A comparison with SLMed bulk Nitinol samples evidenced that the scanning strategy, adopted for the realization of lattice structures, could promote large variations in microstructure, provoking irregularities in the characteristic phases, typical of this functional alloy. It was found that strong texture could be detected in the nodes of the lattice samples, while the reference bulk samples revealed more uniform microstructure orientation, depending on different thermal histories during the SLM process, which did not cause sensible Ni loss.

2. Experimental

The chosen lattice structures were based on a tetragonal diamond-like geometry (strut diameter and length of 1 mm and 2.5 mm, respectively) and characterized by a relative density of 22% with respect to full dense parts. The samples, having a size of 10 mm × 30 mm × 10 mm (see Figure 1), were produced from Ni50.8Ti49.2 (at.%) powder, having a size approximately in the range 5–50 µm, with an SLM system (mod. AM400 from Renishaw, New Mills, Kingswood, Wotton-under-Edge GL12 8JR, UK). The main process parameters, which were investigated elsewhere [17], are listed in Table 1. As a reference, bulk samples (6 mm in height and 3 mm in diameter) were printed using equivalent parameters. Lattice and bulk samples were realized with contour and meander scanning strategy, respectively.

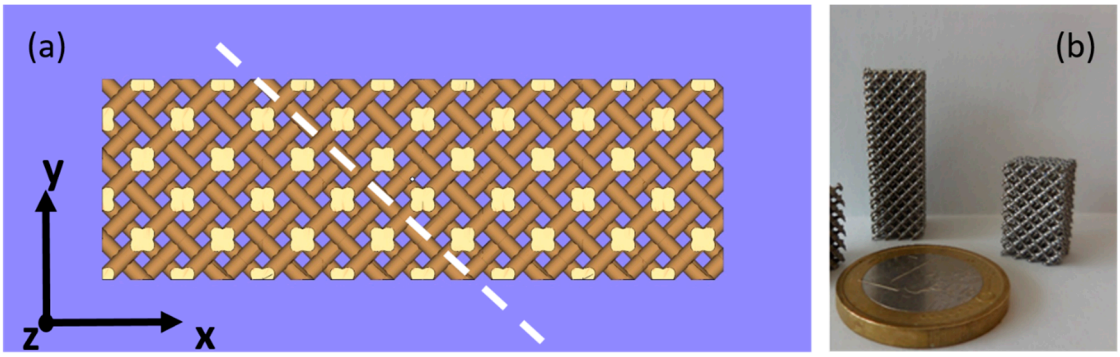

Figure 1. Schematic of the lattice structure, built onto the building platform (**a**), highlighting the building direction (z) containing section where electron backscatter diffraction (EBSD) analysis was performed, and NiTi lattice samples (**b**).

Table 1. Process parameters used for printing Nitinol lattice structure and bulk samples.

Parameters	Values
Power	75 W
Exposure time	75 µs
Atmosphere	Argon
Layer thickness	30 µm
Hatch distance	50 µm
Point distance	50 µm
Laser spot size	65 µm

X-ray computed tomography (CT) was performed on a prismatic portion of a sample, using an XTH225–ST system (Nikon, Leuven, Belgium), having an x-ray gun of 225 kV and a 16-bit flat-panel Varex 4343CT as a detector, to highlight the defects within the entire volume of the sample. The following settings were used for the measurements: (i) voltage of 154 kV; (ii) 7 mm as the resolution of the detector; (iii) 105 min as scanning time.

The samples were characterized in the as-built condition. Differential scanning calorimetry (DSC) was performed on small specimens, about 30 mg in weight, cut with a diamond saw from the built parts: a complete thermal cycle in the (−100 °C; 150 °C) temperature range with heating/cooling rate of 10 °C/min was carried out using a DSC (mod. SSC 5200 by Seiko Instruments, Chiba, Japan). The microstructure was investigated through scanning electron microscopy, coupled with electron backscatter diffraction (EBSD) and energy-dispersive x-ray spectroscopy (EDXS) on the XY view for both the samples (FEG-SEM SU70 from Hitachi, Chiyoda, Japan, equipped with EBSD and EDXS systems from Thermo Scientific, Waltham, MA, USA); moreover, the lattice structure was also analyzed in a section parallel to the building (Z) direction and lying at 45° with respect to the XY plane, as reported in Figure 1 in dashed line. Sections were included in graphite-loaded hot mounting resin, and metallographic surfaces with a final colloidal silica finishing were prepared. Mechanical uniaxial compression tests were performed by means of an MTS 2/M machine (MTS Systems Corporation, Eden Prairie, MN, USA), equipped with an extensometer, at a strain rate of 0.01 min^{-1}. Eight complete loading and unloading cycles, up to 10% in strain, were carried out at room temperature (RT). Prior to testing, all the samples were heated up to 70 °C and then cooled to RT to allow the characterization of the samples in the same condition and to evaluate recoverable strain after unloading.

3. Results and Discussion

A CT scan performed on the lattice structure for analyzing the internal defects is reported in Figure 2. In detail, a representative cross-section of the lattice structure, observed along the XY plane, is shown in Figure 2a. It can be seen that the porosity had no preferential distribution within the nodes. This fact should depend on the scanning strategy adopted during the SLM process: the contour strategy implied an ellipsoidal path of the laser beam from the center to the border of the lattice element; therefore, the best degree of homogeneity on the overlapping of adjacent liquid pools could be reached, as also reported in other works [18]. The analysis of the defects revealed that the defect size ranged between 30 μm and 250 μm, except few larger defects (see Figure 2b), and the sphericity of the main fraction of the defects was in the 0.45–0.7 range. As discussed in previous works [17,19], this behavior suggested that the energy irradiated by the laser beam to the powder bed was sufficient for producing high-density samples.

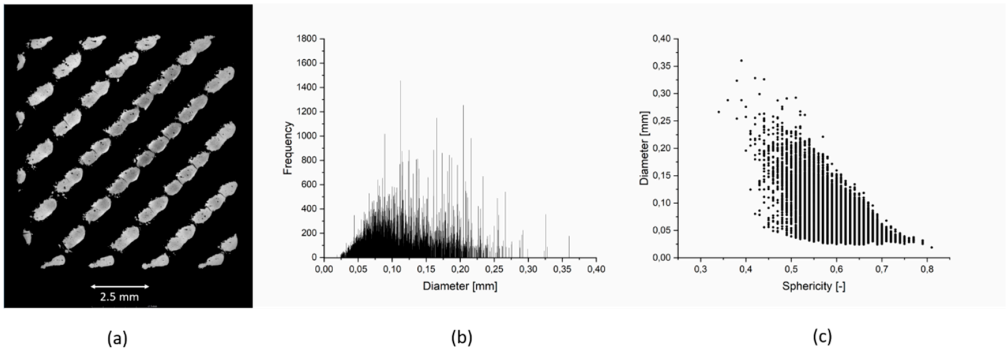

Figure 2. Computed tomography (CT) analysis of the NiTi SLMed structure: cross-section in the XY view (**a**), frequency- diameter (**b**), and diameter-sphericity (**c**) trend.

DSC scans of the lattice and bulk samples are shown in Figure 3, while the characteristic temperatures of the MT (austenite start, peak and finish temperatures, As, Ap and Af, and martensite

start, peak and finish temperatures, Ms, Mp and Mf) and the corresponding heats exchanged ($H_{A\rightarrow M}$ and $H_{M\rightarrow A}$) are listed in Table 2.

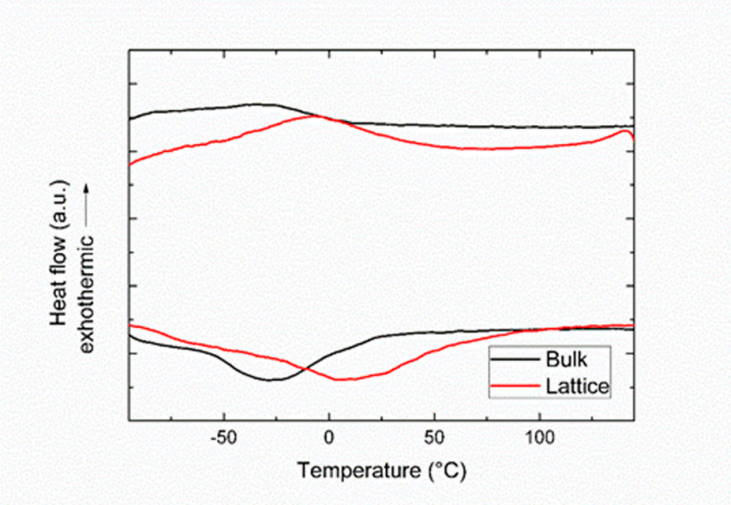

Figure 3. DSC (differential scanning calorimetry) scans of the lattice and bulk samples.

Table 2. Characteristic temperatures of the martensitic transformation (MT) measured for the lattice and bulk samples.

Sample:	As (°C)	Ap (°C)	Af (°C)	$H_{M\rightarrow A}$ (J/g)	Ms (°C)	Mp (°C)	Mf (°C)	$H_{A\rightarrow M}$ (J/g)
Lattice	−47	9	76	10.5	44	−5	−52	7.5
Bulk	−61	−22	30	5.4	11	−28	−86	4.0

Due to the same fluence being used during the SLM process (127 J/mm^3), the increase of temperatures of the martensitic transformation in the lattice sample should reasonably due to the presence of residual stresses: this was in good agreement with the Clausius–Clapeyron equation for shape memory alloys. In fact, the lattice structure was realized through a contour scanning strategy, which was dedicated to thin parts, but also caused higher heat accumulation, due to the laser scanning on an almost circular path. On the contrary, the bulk sample was produced using the meander scanning strategy, which promoted subsequent heating/cooling cycles when the laser beam moved along parallel lines. More intense heat accumulation could lead to slower cooling rates; therefore, grain growth was favorite. Additionally, it could be also mentioned that higher heat accumulation could favor Ni loss, as well as the generation of residual stresses, which are typical of the SLM process, and this resulted in an increase in the temperatures of the MT.

EBSD analyses performed on the XY section of the two specimens are reported in Figure 4. Indexing was performed according to the body-centered cubic austenite. Orientation image micrographs (OIM), calculated for the normal direction of the section (i.e., the building direction (BD) for XY section like the proposed ones), inverse pole figures (IPF), calculated for the normal direction, and (100) pole figures (PF) were reported, respectively. Two main differences between lattice and bulk specimen were well apparent.

The lattice showed (see Figure 4a) the presence of not-indexed (black areas), that could be ascribed to localized martensite, and a not uniform texture; the latter visualized as a more reddish center and randomly colored border regions in OIM of Figure 4b. On the contrary, the bulk specimen (see Figure 4d) showed a more homogeneous microstructure, with a faint (100) texture aligned with BD.

The non-homogeneous texture of the lattice specimen is highlighted in Figure 5. IPFs calculated on the two areas demonstrated that a sharp (100) texture parallel to the BD was present in the center of the section, while a more random texture was observed near the contour. Analyses performed on BD

sections and at higher magnification allowed to partly clarify the origin of both not-indexed regions and texture differences. Columnar grains with (100) texture were mostly developed in the middle of the nodes that had the shape of ligaments built parallel to BD. Contour grains in the struts tended to grow in a more bent direction due to the different spatial thermal gradient experienced by the material in these regions. Equiaxed grains were also present, whose formation could be ascribed to the different intensity of the thermal gradient with respect to the internal regions. A different heat extraction close to the borders was likely due to the surrounding powder—not melted by the laser beam—which had a thermal conductivity lower than the consolidated material.

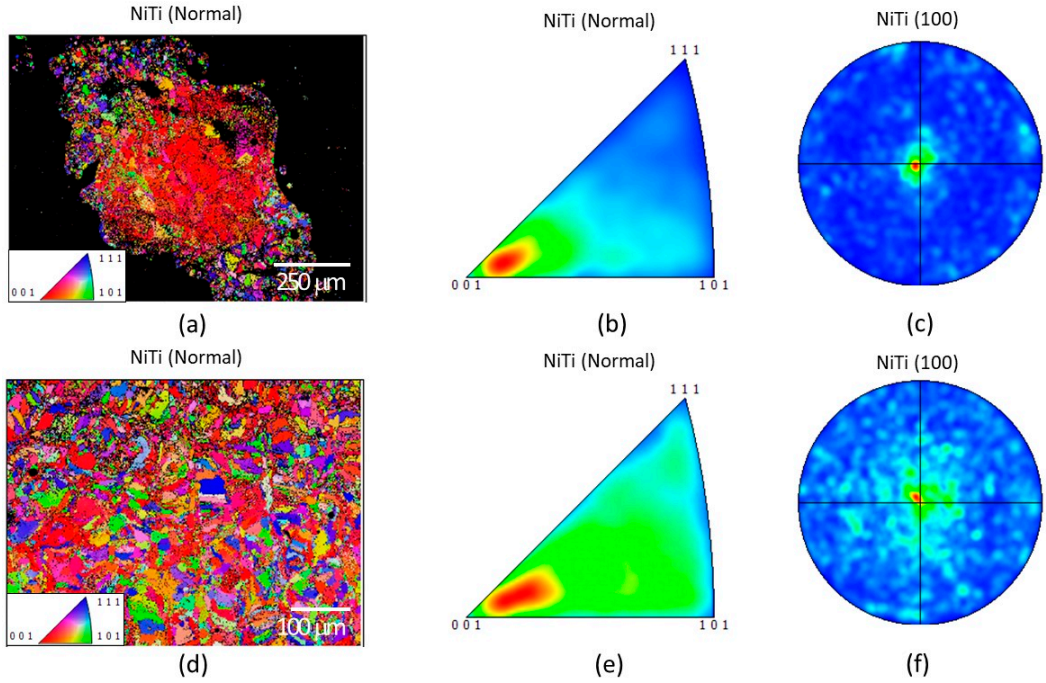

Figure 4. EBSD results on XY section of the lattice (**a**–**c**) and bulk (**d**–**f**) samples, analyzed with orientation image micrographs (OIM) related to building direction (BD), inverse pole figures (IPF), and pole figures (PF) of the analyzed areas, respectively.

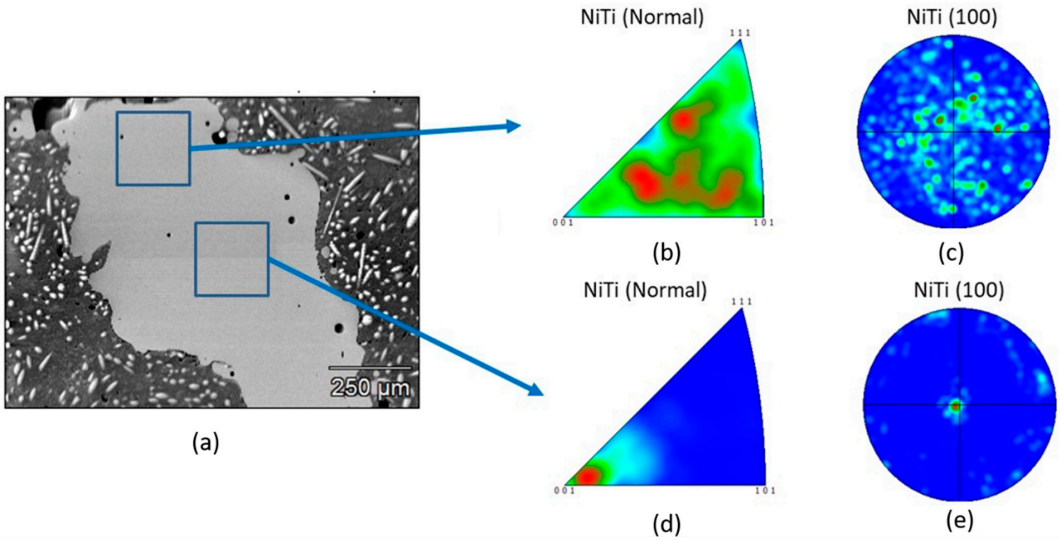

Figure 5. SEM-BSE micrograph acquired on the XY section (**a**). IPF and PF of two regions were reported: (**b**,**c**) region close to the border and (**d**,**e**) central part of the lattice structure.

Not indexed regions, i.e., martensitic areas (see Figure 6c), seemed to well correspond to stress concentration regions, namely, the connection volume between the struts and nodes, as well as the upper surface of nodes. Consequently, they possibly correspond to the presence of bands of stress-induced martensite (SIM) [2,3]. This hypothesis was supported by the fact that the solidification stresses were accumulated in the joint between two or more bridges (massive parts). On the contrary, the extreme parts of the lattice structure, standing alone and free to deform, were able to relax the stresses induced during the rapid solidification, and they reasonably did not exhibit any SIM, as shown in Figure 6. In fact, EBSD performed on the lattice part indicated that only austenite could be detected, and no martensite was present in the formed columnar struts.

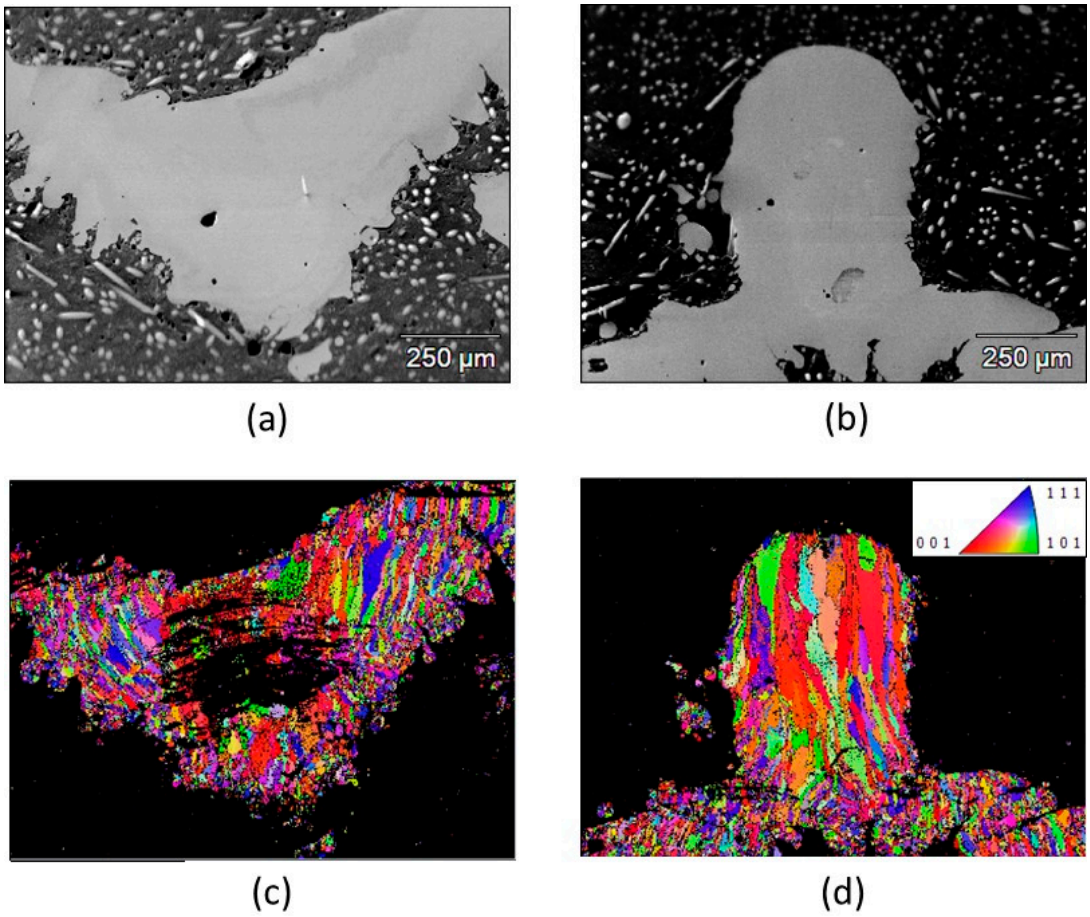

Figure 6. EBSD analyses on the BD section of lattice, involving a node and concurrent struts (**a**,**c**) and an extreme part of the lattice structure (**b**,**d**). a, b Secondary electron reference micrographs, c, d—OIM related to BD.

Moreover, higher magnification analyses in the lattice structure revealed the ideal continuity of austenite grains above and below martensitic regions, as represented in Figure 7. EDX analyses of lattice, performed on areas of about 200 µm × 200 µm, didn't reveal any statistically significant compositional differences. On the contrary, a small variation in Ni content was observed at the micrometric scale (see Figure 7d–f).

It is worth noting that, in this case, the EDXS analyses were indeed performed close to their detectability limit. All these considerations led to the conclusion that wide areas of stress-induced martensite were present in the lattice structure. In terms of comparison, the compositional analysis performed on the bulk sample revealed that Ni content was 50.9 ± 0.15, measured in atomic percentage, and the average Ni content in the lattice samples was 50.95%; thus, no significant compositional

variations were detected between lattice and bulk specimens due to the use of equivalent process parameters [20].

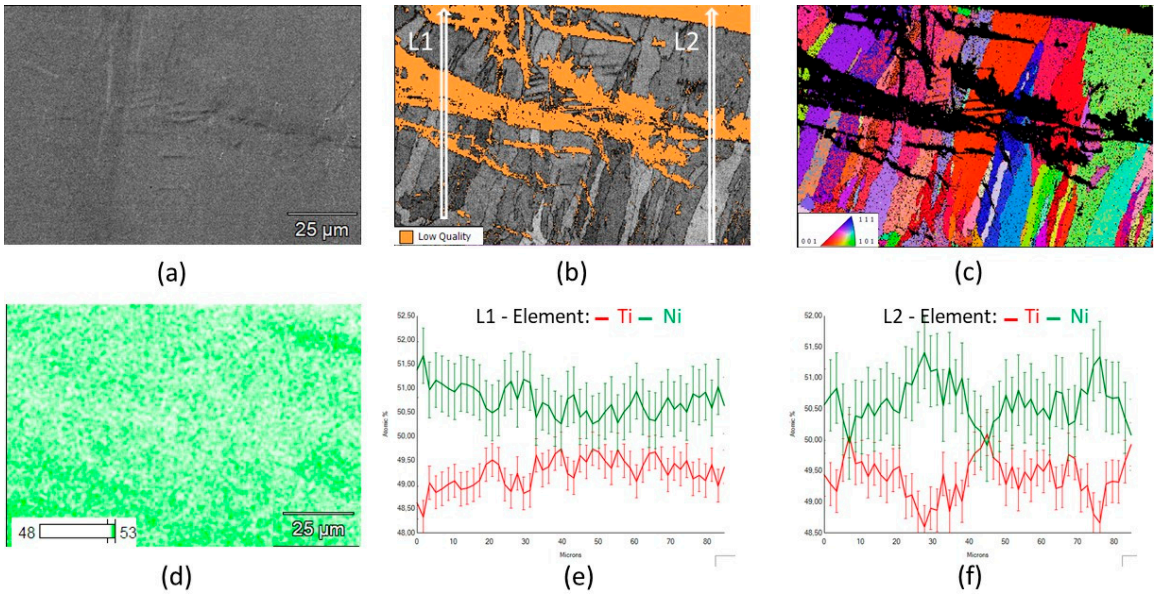

Figure 7. Higher magnification EBSD/EDXS analysis on BD section: (**a**) reference secondary electron micrograph, (**b**) pattern quality map, (**c**) OIM related to BD, (**d**) EDXS Ni distribution map, (**e**,**f**) extracted line analyses of line 1 and 2 in Figure 6b.

The mechanical behavior of the Nitinol lattice structure under subsequent loading/unloading cycles under compression is shown in Figure 8a. In terms of comparison, the mechanical behavior of the bulk sample tested in compression, thoroughly described in [17], is shown in Figure 9. During deformation, the reached stresses were obviously much lower than the ones which could be expected in a bulk sample since they were computed considering the sample as if it was "fully dense", according to the widespread agreement [21]. Recovered strains (Figure 8c) increased almost linearly with imposed deformation. In particular, an interesting value of 4.5% was reached for a 10% imposed deformation. At large deformations (higher than 7%), the recovery abilities inherent to the geometry's low stiffness were likely to start playing an overwhelming role. At the same time, the beginning of the lattice densification gave rise to a plateau-like behavior. It should be noted that the bulk samples appeared to allow a higher degree of recovery, at least up to 7% deformation. This behavior, which might seem to be counterintuitive at first, was explained by considering that, as highlighted by EBSD analysis, trabecular structures contained a higher amount of martensite in the as-built state. Moreover, it was likely that the stress concentration acting at each node of the structure was able to induce martensite at early stages and readily plastically deform it, thus preventing the reverse transformation into austenite. In order to have a complete perspective on the mechanical properties of the produced NiTi lattice structures, a sample was deformed in compression up to 4% and 6% and then heated to approximately 80 °C. These temperatures, as shown in Figure 2, laid above the A_f temperature and were, therefore, expected to induce the transformation of the SIM into austenite. In fact, both residual deformations upon unloading (1.72% and 2.75%, respectively) were completely recovered after heating at 80 °C (see Figure 8c).

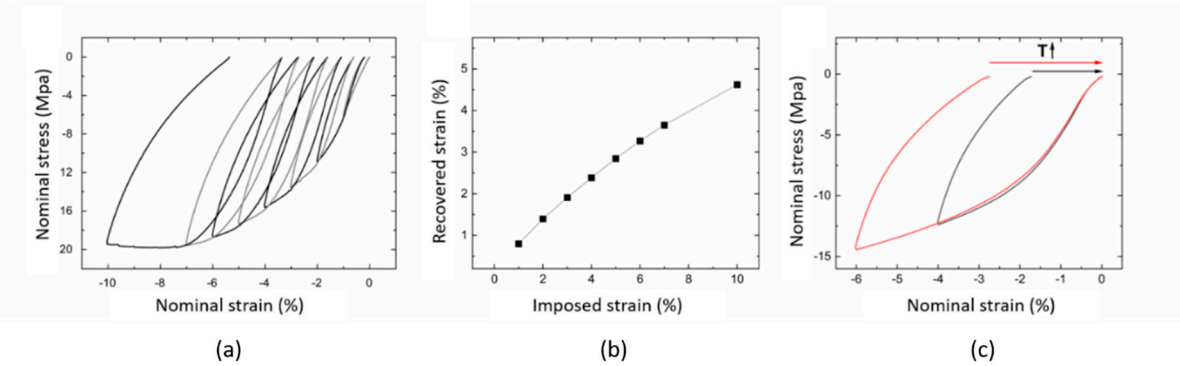

Figure 8. Mechanical behavior under compression of the lattice sample (**a**); the trend of recovered vs. imposed deformation (**b**); strain recovery (**c**).

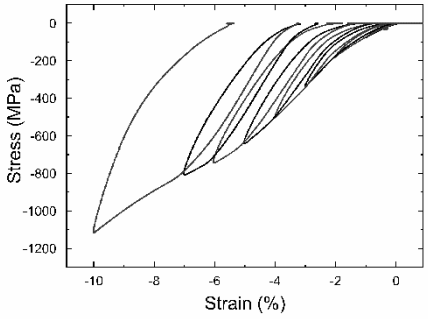

Figure 9. Mechanical behavior under compression of the bulk sample [18].

4. Conclusions

In this work, the microstructure and the mechanical behavior of Nitinol lattice structures, produced by selective laser melting, were studied. It can be highlighted that:

(1) The martensitic transformation of the lattice structure occurred at temperatures slightly higher than the bulk material due to the formed residual stresses;

(2) The lattice structures exhibited nodes with some areas of stress-induced martensite and fully austenitic struts, while the bulk sample was fully austenitic;

(3) Grains were oriented along preferential directions in the lattice structures, while they were more casually oriented in the bulk sample;

(4) Compression behavior of the lattice structure indicated that the recovered strain increased directly proportionally with the imposed strain; moreover, at room temperature, the lattice structure exhibited a partial superelastic response, while residual deformation was recovered after heating up to 80 °C.

Author Contributions: Conceptualization, C.A.B. and A.T.; methodology, C.A.B.; validation, all authors.; formal analysis, C.A.B., J.F. and P.B.; investigation, C.A.B., J.F. and P.B.; resources, A.T.; writing—original draft preparation, C.A.B., J.F. and P.B.; writing—review and editing, all authors; visualization, C.A.B.; supervision, A.T.; project administration, A.T.; funding acquisition, A.T. All authors have read and agreed to the published version of the manuscript.

Funding: This research was funded through Accordo Quadro between CNR and Regione Lombardia, grant number 3866.

Acknowledgments: The authors would like to acknowledge Saes Getters SpA as a supplier of Nitinol powder, Nikon for the support in the Computer Tomography analysis, and Accordo Quadro CNR/Regione Lombardia n. 3866 at 17/07/2015 FHfFC for financial support. The authors would like to thank Nicola Bennato from CNR ICMATE for his support in the experimental activity.

Conflicts of Interest: The authors declare no conflict of interest.

References

1. Tang, Y.; Zhao, Y.F. A survey of the design methods for additive manufacturing to improve functional performance. *Rapid Prototyp. J.* **2016**, *22*, 569–590. [CrossRef]
2. Otsuka, K.; Wayman, C.M. *Shape Memory Materials*; Cambridge Univ. Press: Cambridge, UK, 1998.
3. Otsuka, K.; Ren, X. Physical Metallurgy of Ti-Ni based shape memory alloys. *Prog. Mater. Sci.* **2005**, *50*, 511–678. [CrossRef]
4. Van Humbeeck, J. Non medical applications of shape memory alloys. *Mater. Sci. Eng. A* **1999**, *273*, 134–148. [CrossRef]
5. Duerig, T.; Pelton, A.; Stöckel, D. An overview of nitinol medical applications. *Mater. Sci. Eng. A* **1999**, *273*, 149–160. [CrossRef]
6. Elahinia, M.; Shayesteh Moghaddam, N.; Taheri Andani, M.; Amerinatanzi, A.; Bimber, B.A.; Hamilton, R.F. Fabrication of NiTi through additive manufacturing: A review. *Prog. Mater. Sci.* **2016**, *83*, 630–663. [CrossRef]
7. Saedi, S.; Moghaddam, N.S.; Amerinatanzi, A.; Elahinia, M.; Karaca, H.E. On the effects of selective laser melting process parameters on microstructure and thermomechanical response of Ni-rich NiTi. *Acta Mater.* **2018**, *14*, 552–560. [CrossRef]
8. Speirs, M.; Wang, X.; van Baelen, S.; Ahadi, A.; Dadbakhsh, S.; Kruth, J.P.; Van Humbeck, J. On the Transformation Behavior of NiTi Shape-Memory Alloy Produced by SLM. *Shape Mem. Superelasticity* **2016**, *2*, 310. [CrossRef]
9. Dadbakhsh, S.; Speirs, M.; Van Humbeck, J.; Kruth, J.P. Laser additive manufacturing of bulk and porous shape memory NiTi alloys: From processes to potential biomedical applications. *MRS Bull.* **2016**, *41*, 765–774. [CrossRef]
10. Andani, M.T.; Saedi, S.; Turabi, A.S.; Karamooz, M.R.; Haberland, C.; Karaca, H.E.; Elahinia, M. Mechanical and Shape Memory properties of porous Ni50.1Ti49.9 alloys manufactured by selective laser melting. *J. Mech. Behav. Biomed. Mater.* **2017**, *68*, 224–231. [CrossRef] [PubMed]
11. Fiocchi, J.; Biffi, C.A.; Scaccabarozzi, D.; Saggin, B.; Tuissi, A. Enhancement of the Damping Behavior of Ti6Al4V Alloy through the Use of Trabecular Structure Produced by Selective Laser Melting. *Adv. Eng. Mater.* **2019**. [CrossRef]
12. Demir, A.G.; Previtali, B. Additive manufacturing of cardiovascular CoCr stents by selective laser melting. *Mater. Des.* **2017**, *119*, 338–350. [CrossRef]
13. Funakubo, H. *Shape Memory Alloys*; Gordon and Breach Science Publishers: Amsterdam, The Netherlands, 1987.
14. Nishida, M.; Wayman, C.; Honma, T. Precipitation processes in near-equiatomic TiNi shape memory alloys. *Metall. Trans. A* **1986**, *17*, 1505–1515. [CrossRef]
15. Mahmoudi, M.; Tapia, G.; Franco, B.; Ma, J.; Arroyave, R.; Karaman, I.; Elwany, A. On the printability and transformation behavior of nickel-titanium shape memory alloys fabricated using laser powder-bed fusion additive manufacturing. *J. Manuf. Process.* **2018**, *35*, 672–680. [CrossRef]
16. Bormann, T.; Muller, B.; Schinhammer, M.; Kessler, A.; Thalmann, P.; de Wild, M. Microstructure of selective laser melted nickel-titanium. *Mater. Charact.* **2014**, *94*, 189–202. [CrossRef]
17. Biffi, C.A.; Fiocchi, J.; Bassani, P.; Tuissi, A. Selective Laser Melting of NiTi Shape Memory Alloy: Processability, microstructure and superelasticity. *Shape Mem. Superelasticity* **2020**. Under consideration.
18. Biffi, C.A.; Fiocchi, J.; Ferrario, E.; Fornaci, A.; Riccio, M.; Romeo, M.; Tuissi, A. Effects of the scanning strategy on the microstructure and mechanical properties of a TiAl6V4 alloy produced by electron beam additive manufacturing. *Int. J. Adv. Manuf. Technol.* **2020**, 1–12. [CrossRef]
19. Fiocchi, J.; Biffi, C.A.; Tuissi, A. Selective laser melting of high-strength primary AlSi9Cu3 alloy: Processability, microstructure, and mechanical properties. *Mater. Des.* **2020**. [CrossRef]
20. Shiva, S.; Palani, I.A.; Mishra, S.K.; Paul, C.P.; Kukreja, L.M. Investigation on the influence of composition in the development of Ni-Ti shape memory alloy using laser based additive manufacturing. *Opt. Laser Technol.* **2015**, *69*, 44–51. [CrossRef]
21. Ashby, M.F.; Evans, A.G.; Fleck, N.A.; Gibson, L.J.; Hutchinson, J.W. *Metal Foams: A Design Guide, Butterworth-Heinemann*; United States of America: Boston, MA, USA, 2000.